Driving Force Control for Electric Vehicles: A Survey on Its Origin, Developments, and Future Trends

Binh-Minh Nguyen*a) Member, Yuki Hosomi* Student-member, Tona Sato* Student-member, Yuna Morimoto* Student-member, Tokikazu Mizuguchi* Student-member, Michi Oda** Member, Hiromitsu Toyota*** Member, Sakahisa Nagai* Member, Hiroshi Fujimoto* Senior-member

After 15 years of development, driving force control (DFC) has grown up as a promising research topic in the field of traction control for electric vehicles. In general, DFC has a cascade configuration which consists of a reaction force controller in the outer loop, a wheel speed controller in the inner loop, and an outer-to-inner signal limiter. This configuration allows DFC to accurately track the driving force to its reference on high-friction surface, and effectively prevent the slip phenomenon on low-friction surface. This paper introduces the fundamental philosophy behind the genesis of DFC to explain the advances of DFC in comparison with other two popular traction control strategies, namely, slip ratio control and anti-slip control. The main developments are summarized, followed by a discussion on the future challenges for the study of DFC.

Keywords: electric vehicle, driving force control, disturbance observer, driving stiffness, slip ratio, traction control.

1. Introduction

Thanks to the ability of quick and accurate torque response, various advanced motion control approaches were developed for electric vehicles (EVs) [1]. This paper investigates the most fundamental motion control layer. This is traction control, which is to properly generate the motion between the wheel and the road surface. Traction control methods are categorized into three main groups: slip ratio control (SRC), anti-slip control (ASC), and driving force control (DFC).

The SRC [2], [3] has been trapped by some practical challenges. First, accurate estimation of slip ratio and tuning of slip ratio reference in real-time are nontrivial. Second, it is difficult to integrate SRC with the upper-layer motion controller. For instance, the output of the direct yaw moment control layer would be driving force instead of slip ratio. Third, by using SRC, the slip ratio appears in the cost function of the energy optimization problem [4], thereby increasing the complexity of optimal torque distribution in real-time. Besides, ASC was developed based on disturbance observer (DOB) with a nominal model from motor torque to wheel velocity. The typical ASC are zero-slip model following control [5] and maximum transmissible torque estimation [6]. ASC is transparently simple, and it does not require the chassis velocity. Unfortunately, ASC is merely a rough traction which cannot guarantee accurate tracking of slip ratio and/or driving force.

With respect to the above discussion, this paper focuses on the DFC, which was originally invented by Fujimoto research group [7]. DFC was proposed based on two main pillars. (i) The driving force can be estimated accurately using the motor torque and wheel velocity. (ii) The slip ratio can be used as a control variable of the driving force. Consequently, DFC was designed with a cascade configuration which consists of a reaction force controller in the outer loop, a wheel speed controller in the inner loop, and an outer-to-inner limiter that addresses the friction limit circle. Thanks to the cascade configuration, DFC overcomes almost all the demerits of SRC and WSC. It provides accurate tracking of the driving force on the high friction surface, and effectively prevents the slip phenomenon on low friction surface. The motion of the vehicle body is generated by the friction force between the wheel and road surface. Therefore, it is straightforward to integrate DFC with various upper-layer motion controllers, such as vertical vibration suppression, yaw-rate control, roll angle control, and range extension control.

Until now, DFC has been a real and promising topic in the field of traction control [7]-[23]. However, the literature of DFC has not been summarized systematically. Thus, this paper is to contribute a thorough survey on DFC by highlighting its origin and introducing some main developments for both in-wheel-motor EVs (IWM-EVs) and onboard-motor EVs (OBM-EVs). Furthermore, this paper discusses the future trends and challenges in the study of DFC.

2. The genesis of DFC

2.1 Vehicle model As shown in Fig. 1, the motion of the vehicle is described by the following equations:

$$m\dot{v}_x = F - F_d \quad \cdots\cdots (1)$$

$$J_w\dot{\omega} = T - rF \quad \cdots\cdots (2)$$

where m is the vehicle mass; v_x is the vehicle velocity; F is the driving force; and F_d is the summation of air and rolling resistance. Besides, ω is the wheel's rotational velocity; J_w and r are the inertia and radius of the wheel, respectively; T is the motor torque; and Z is the vertical force. The slip ratio is defined as:

$$\lambda = \frac{r\omega - v_x}{\max\{r\omega, v_x, \varepsilon\}} \quad \cdots\cdots (3)$$

a) Correspondence to: Binh-Minh Nguyen.
E-mail: nguyen.binhminh@edu.k.u-tokyo.ac.jp
* The University of Tokyo, Department of Advanced Energy.
** Ono Sokki Co., Ltd., *** Mitsubishi Motors Corporation.

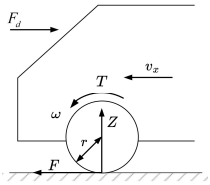

Fig. 1. Single wheel model.

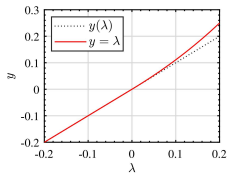

Fig. 2. y and λ map.

where ε is a small positive number that prevents division by zero. There exists a nonlinear relationship between F and λ, and it is commonly described by Pacejka's magic formula [24].

2.2 Ideas of DFC The driving force can be controlled by a feedforward approach, i.e., $T = rF^*$ where F^* is the reference force. However, feedforward control cannot eliminate the tracking error between F and F^*. Therefore, feedback control has been developed based on the following ideas:

(i) Force estimation: From (2), the driving force observer (DFO) is designed as follows with the first-order low-pass filter $Q(s)$.

$$\hat{F}(s) = Q(s)\left[T(s) - J_w s\omega(s)\right]/r \quad \cdots\cdots (4)$$

(ii) Cascade force control: Define the variable

$$y = \begin{cases} \lambda/(1-\lambda) & (r\omega \geq v_x) \\ \lambda & (r\omega < v_x) \end{cases} \quad \cdots\cdots (5)$$

For small slip ratio region, y is almost close to λ (Fig. 2). Thus, F can be linearized as $F \approx D_s\lambda \approx D_s y$ where D_s is the driving stiffness. Consequently, y can be used as a control variable to control the driving force. We let y_c^* be output of the reaction force controller (RFC). For the purpose of slip prevention, y_c^* should be limited by a signal-limiter (SL) with the upper-bound $+y_{max}$ and the lower-bound $-y_{max}$. Let y^* be the output of the SL, the reference wheel velocity (RWV) is calculated as:

$$\omega^* = (1+y^*)v_x / r \quad \cdots\cdots (6)$$

Then, a wheel velocity controller (WVC) is implemented to track the wheel velocity with the reference value (6). Based on the above ideas (i) and (ii), the DFC system was established as in Fig. 3.

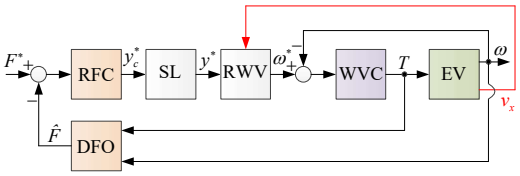

Fig. 3. Block diagram of DFC system.

2.3 Discussion The original version of DFC [7] was proposed by Yoshimura and Fujimoto in 2011. The method was implemented for an IWM-EV with an integral RFC and a proportional-integral WVC. WVC and RFC were designed using pole placement with respect to the nominal transfer functions from T to ω and y to F, respectively. The SL was fixed at a small value, such as 0.1. Consequently, the original version of DFC triggered four essential issues.

(1) Update the boundary of the SL in accordance with the change of road friction coefficient.

(2) Integrate DFC with the upper-layer motion controllers.

(3) Analyze the stability of the overall DFC system.

(4) Extend the original DFC to OBM-EVs.

Especially, the last question raises a new research direction. Due to the existence of differential gears and shafts, OBM-EV has a more complex mechanism in comparison with the IWM-EV. Thus, the driving force must not be estimated using a simple DFO as for IWM-EV. In addition, the dynamical system from T to ω should be treated as a complex transfer function of high order. Simply using a proportional-integral controller is not enough to guarantee good control performance.

3. Development of DFC

Table 1 is a summary of the development of DFC to tackle the aforementioned issues. Due to the limitation of paper space, this paper only introduces several recent achievements.

3.1 DFC based integrated motion control system Following the work of Maeda et al [10], the block diagram of the integrated control system is established as in Fig. 4. The system has a hierarchically decentralized configuration with yaw-rate

Table 1. A summary of DFC development.

Research issue	Proposal	Comment	Ref. No.
(1) Update the boundary of SL in accordance with road friction coefficient change	Derivation of the maximum slip ratio using brush tire model and sideslip angle.	• Merit: Cornering force maximization. • Challenge: Accurate estimation of sideslip angle.	(8)
	Using onboard camera image processing to determine the road friction coefficient and maximum slip ratio.	• Merit: Vehicle model is not required. • Challenge: Integration of vision-based approach with dynamics-sensor-based approach.	(9)
(2) Integrate DFC with the upper-layer motion controllers	DFC based yaw-rate control to maintain the straight direction with the minimization of sum of squares of slip ratios.	• Merit: Allow additional objective by force distribution. • Challenge: Variable SL was not considered.	(10)
	DFC based yaw moment control when the vehicle corners on the low friction surface.	• Merit: Enhance the yaw-rate tracking performance. • Challenge: Variable SL was only applied to one wheel.	(11)
	DFC based range extension control.	• Merit: Integration DFC with energy optimization. • Challenge: Robustness to energy model parameter?	(12)
(3) Analyze the stability of the overall DFC system	Represent the system as the feedback connection of the SL and an equivalent transfer function for absolute stability analysis.	• Merit: Alleviate the design burden by utilizing the graphical test of system stability. • Challenge: + Robust stability analysis of the system including DFC and upper-layer controllers. + Extension to the general OBM-EVs.	(13), (14)
	Represent the system using a rank-1 physical interaction matrix and a generalized frequency variable.		(15)
(4) Extend the original DFC to OBM-EVs	WVC design based on two-inertia modeling of the mechanism from motor torque to wheel velocity.	• Merit: Vibration suppression of driving shaft. • Challenge: Accurate estimation of driving force, lack of feedforward controller.	(16), (17), (18)
	Frequency domain model identification to design feedforward driving force controller and a transformer from wheel velocity reference to motor velocity reference.	• Merit: Systematic approach to feedforward control. • Challenge: Stability and robustness of the overall system under parameter uncertainties.	(19)
	Feedforward and feedback control design for drive shaft vibration suppression based on frequency domain analysis.	• Merit: Improve the performance of the two input two output motor drive system. • Challenge: Stability analysis of overall system	(20)
	Adaptive driving force observer by combining state observer and RLS parameter identification.	• Merit: Adaptive to viscous friction coefficient change. • Challenge: Stability	(21)
	Cascade feedforward controller for outer-loop (force control) and inner-loop (motor velocity control) with absolute stability analysis of the overall DFC system.	• Merit: Alleviate the design burden while improving control performance. • Challenge: Real vehicle experiments are required.	(22)
	Design of adaptive SL and DFC based yaw moment control for OBM-EV with two-input two-output motor drive.	• Merit: Enhance the cornering of OBM-EV. • Challenge: How to accurately estimate the optimal slip ratio when tire slip angle is zero.	(23)

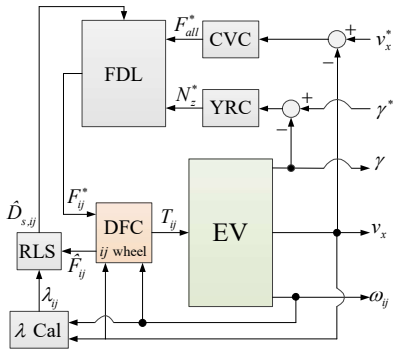

Fig. 4. DFC based integrated motion control system.

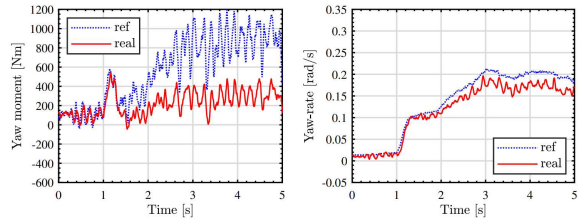

(a) With fixed SL.

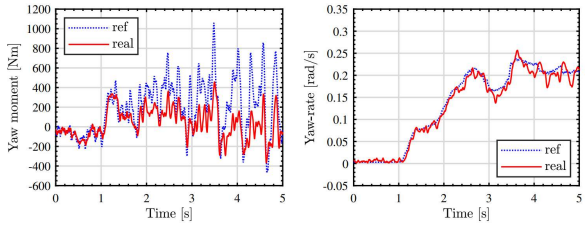

(b) With adaptive SL.

Fig. 5. Experimental results of DFC based yaw-rate control.

controller (YRC) and chassis velocity controller (CVC) in the upper-layer, and a bunch of DFCs in the lower-layer. YRC outputs the yaw moment command N_z^*, and CVC outputs the total driving force command F_{all}^*. The index ij represents the location of the wheels: front-left (fl), front-right (fr), rear-left (rl) and rear-right (rr). Let the tread bases of the front wheels and rear wheels be d_f and d_r, respectively. The force distribution law (FDL) must satisfy the following constraints:

$$\begin{bmatrix} 1 & 1 & 1 & 1 \\ -\frac{d_f}{2} & \frac{d_f}{2} & -\frac{d_r}{2} & \frac{d_r}{2} \end{bmatrix} \begin{bmatrix} F_{fl}^* & F_{fr}^* & F_{rl}^* & F_{rr}^* \end{bmatrix}^{\mathrm{T}} = \begin{bmatrix} F_{all}^* \\ N_z^* \end{bmatrix} \quad \cdots\cdots (7)$$

With four wheels, it is possible to optimize an additional cost function, such as the total workload, the total motor input power [4]. Maeda et al [10] considered the sum of squares of slip ratios:

$$\mathcal{L} = \sum_{ij} \left(F_{ij}^* / D_{s,ij}^* \right)^2 \quad \cdots\cdots (8)$$

To this end, a recursive least square (RLS) algorithm is implemented to identify the driving stiffness $D_{s,ij}$ in real-time. The optimal solution of $\{F_{ij,opt}^*\}$ is obtained using Lagrange multiplier method. The control system in Fig. 4 can be further improved by implementing for each DFC an adaptive signal limiter (ASL), which has been studied by Fuse et al [8], Ueno et al [9], and Sato et al [23]. Fig. 5 shows the cornering test results on low friction surface. Transparently, by utilizing the ASL that updates y_{max} in real-time, the difference between the desired and real yaw moments is reduced. Consequently, the tracking performance of yaw-rate with its reference value is successfully enhanced.

3.2 New DFC with absolute stability analysis The DFC in Fig. 3 still have some demerits. First, it requires accurate measurement of vehicle chassis velocity to calculate the wheel velocity reference. Second, it is not provided with any theoretical result to guarantee system stability. To overcome such issues, a new DFC configuration has been proposed recently [13] [14] [15]. As shown in Fig. 6, the RFC is designed as an anti-windup controller, and it directly outputs the wheel speed reference. The chassis velocity, therefore, is only used to update the SL (wheel velocity limiter). Furthermore, it can be obtained a transfer function $G(s)$ from ω^* to $\hat{F}$. Consequently, we can represent the system in Fig. 6 as the feedback connection of the SL and a transfer function $H(s)$:

$$H(s) = G(s)\frac{K_{fp}s + K_{fi}}{s + K_{awu}K_{fi}K_{fp}^{-1}} - \frac{K_{awu}K_{fi}K_{fp}^{-1}}{s + K_{awu}K_{fi}K_{fp}^{-1}} \quad \cdots\cdots (9)$$

Practically speaking, SL is bounded by the sector $[\alpha, \beta]$ where the values α, β are obtained from experiment (Fig. 7a). Following the Circle criterion for absolute stability [25], the design condition of the DFC is stated as follows (see Fig. 7b):

Design condition: The control gains of the DFC are chosen such that the Nyquist plot of $H(j\omega)$ does not enter the disk $D(\alpha, \beta)$ which intersects with the real axis at $(-\alpha^{-1}, 0)$ and $(-\beta^{-1}, 0)$.

Fig. 8 demonstrates the experimental evaluation of the new DFC. Several methods were conducted for comparison: Method 1 (Feedforward force control), Method 2 (Anti-slip control by DOB). Methods 3-1 and 3-2 (New DFC with integral RFC), Method 3-3 (New DFC with anti-windup proportional-integral RFC). It can be seen that the new DFC with anti-windup RFC shows the best control performance. It reduces the vibration of the driving force in comparison with other methods. Especially, it does not suffer the large overshoot as the vehicle returns to the high friction surface from low friction surface. Even if the chassis velocity measurement has an error of 10%, the good control performance is still maintained successfully. The proposed DFC (Method 3-3) decreases the overshoot by 70% in comparison with Method 3-1.

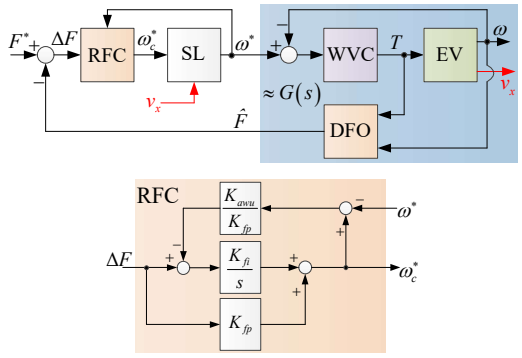

Fig. 6. Block diagram of the new DFC system.

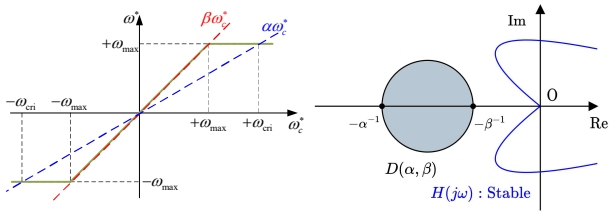

(a) Sector-bound of SL. (b) Circle criterion.

Fig. 7. Setting for absolute stability analysis.

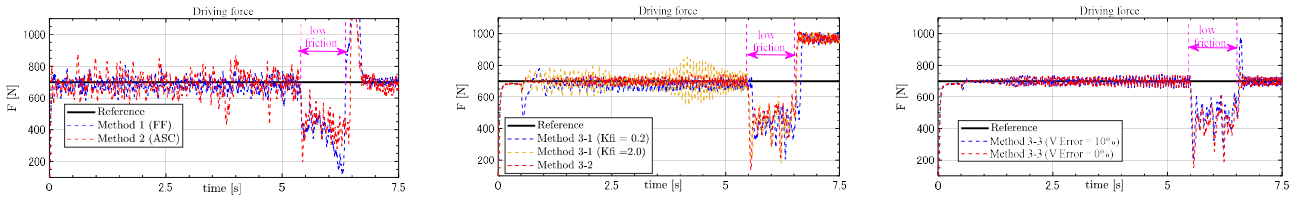

Fig. 8. Experimental evaluation of the new DFC system.

3.3 DFC for OBM-EVs Compared with the fellow IWM-EVs, OBM-EVs have much more complex drive systems, as can be seen in Figs. 9a and b. Let g_{md} be the gear reduction ratio, the torque T_m and angular velocity ω_m of the motor are transformed to the torque T_M and angular velocity ω_M at the ring gear as: $T_M = g_{md}^{-1} T_m$ and $\omega_M = g_{md}\omega_m$. The equations that describe the rotational motion of the motor (M) and wheel load (L) are expressed as follows [16]:

$$J_M \dot{\omega}_M = T_M - B_M \omega_M - K_s \theta_s \quad \cdots\cdots (10)$$

$$J_{L0} \dot{\omega}_L = K_s \theta_s - B_L \omega_L - rF \quad \cdots\cdots (11)$$

$$\theta_s = \begin{cases} \theta_S - \theta_b & (\theta_S > \theta_b) \\ 0 & (-\theta_b \le \theta_S \le \theta_b) \\ \theta_S + \theta_b & (\theta_S < -\theta_b) \end{cases} \text{ with } \theta_S = \int (\omega_M - \omega_L) dt \quad (12)$$

where $\omega_M, J_M, B_M, \omega_L, J_{L0}, B_L$ are the rotational velocities, equivalent inertias and viscous friction coefficient of the motor side and wheel load side, respectively. K_s is the drive shaft rigidity. Equation (12) represents the backlash of the differential gear where θ_b is the boundary value of the deadband. Based on the above equations and Figs. 9a and b, the OBM-EV can be equivalently modelled as a two-inertia system in Fig. 9c.

Remark: The two-inertia model shows that DFC for OBM-EV is different to DFC for IMW-EV in the following senses: (i) The DFO for OBM-EV must take into account both inertia and viscous friction terms. Especially, the DFO should address the uncertainties of the physical parameters. (ii) A dynamical transformer must be designed to transform from wheel velocity reference to motor velocity reference and guarantee system stability. In addition, higher-order velocity controllers should be considered to improve system performance. (iii) In case of IWM-EV, the feedforward force control is merely $T = rF^*$. However, the feedforward force control of OMB-EV would be a real transfer function to address the drivetrain mechanism.

With respect to the above remark, the general block diagram of the DFC for OBM-EV is established as in Fig. 10. The system consists of the reaction force controller (RFC), feedforward force controller (FFC), adaptive-driving force observer (A-DFO), signal limiter (SL), a functional block for reference wheel velocity (RWV), a transformer from wheel to motor velocity reference $G_{L\to M}$, and a motor velocity controller (MVC).

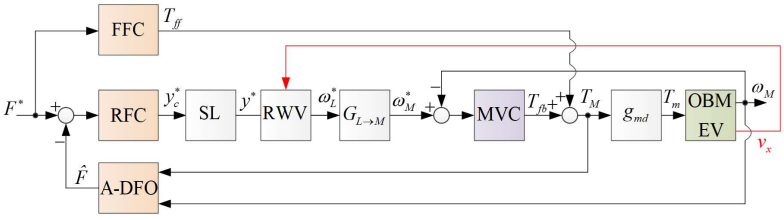

Fig. 10. General configuration of DFC for OBM-EV.

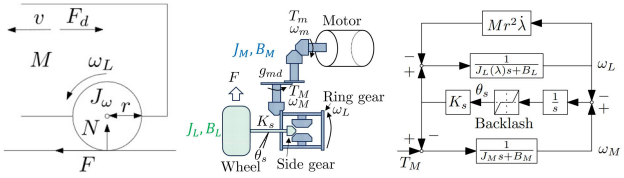

(a) Vehicle and wheel. (b) Drivetrain. (c) Two-inertia model.

Fig. 9. Modeling of OBM-EV.

This subsection introduces the design of A-DFO with the structure in Fig. 11. Summarizing (10) and (11) under the reasonable assumption that ω_M and ω_L almost equal, the following dynamical equation is obtained:

$$J_{ML} \dot{\omega}_M = -B_{ML} \omega_M - rF + T_M \quad \cdots\cdots (13)$$

where $J_{ML} = J_M + J_{L0}$, $B_{ML} = B_M + B_L$. From (13), the state space model is established as follows:

$$\begin{cases} \dot{X} = AX + BU \\ Y = CX \end{cases} \quad \cdots\cdots (14)$$

where $X = \left[\omega_M \;\; F\right]^{\mathrm{T}}$, $Y = \omega_M$, $U = T_M$

$$A = \begin{bmatrix} -\dfrac{B_{ML}}{J_{ML}} & -\dfrac{r}{J_{ML}} \\ 0 & 0 \end{bmatrix}, B = \begin{bmatrix} \dfrac{1}{J_{ML}} \\ 0 \end{bmatrix}, C = \begin{bmatrix} 1 & 0 \end{bmatrix}$$

Assuming that B_{ML} is the uncertain parameter, we can express from (13) the relationship $\varphi^{\mathrm{T}}\theta = \gamma$ where $\theta = B_{ML}$, $\varphi^{\mathrm{T}} = \omega_M$, $\gamma = T_M - J_{ML}\dot{\omega}_M - \hat{F}$. Thus, B_{ML} can be estimated using recursive least square (RLS) algorithm as follows:

$$\begin{aligned} \hat{\theta}_k &= \hat{\theta}_{k-1} + K_k \left(\gamma_k - \varphi_k^{\mathrm{T}} \hat{\theta}_{k-1}\right) \\ K_k &= P_k \varphi_k \left(\sigma + \varphi_k^{\mathrm{T}} P_{k-1} \varphi_k\right)^{-1} \\ P_k &= \sigma^{-1} \left(1 - K_k \varphi_k^{\mathrm{T}}\right) P_{k-1} \end{aligned} \quad \cdots\cdots (15)$$

where σ is the forgetting factor which is slightly close to 1. A state observer is designed based on (14) using pole placement, and its matrices are updated every estimation period using $\hat{B}_{ML}$. In other words, the state observer and parameter identification establish a closed loop. To guarantee the convergence performance of A-DFO, the state observer's gains and the RLS's forgetting factor should be selected for faster convergence of driving force while considering the effect of noises.

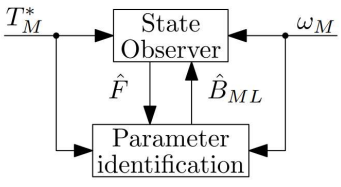

Fig. 11. Adaptive driving force observer (A-DFO).

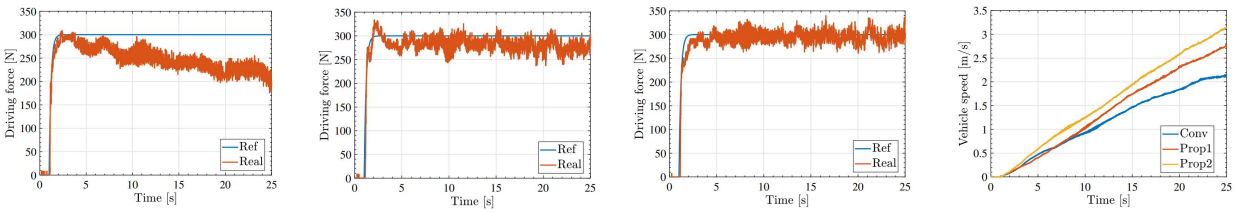

(a) Conventional. (b) Proposal 1. (c) Proposal 2. (d) Comparison of vehicle velocity.

Fig. 12. Experimental results of DFC for OBM-EV.

For comparison, three methods were performed:

Conventional DFC: The DFO is designed similarly to that of IWM-EV without considering the viscous friction term; and the MVC is merely a PI controller.

Proposal-1: The DFO is designed using the state space model (13) using a nominal viscous friction coefficient; and the MVC is a PID controller with a lead-compensator.

Proposal-2: The DFO is designed using the adaptive structure in Fig. 11; and the MVC is a PID controller with lead-compensator.

$$C_{PID-Lead} = \left(K_p + \frac{K_i}{s} + \frac{K_d}{\tau_d s + 1}\right)\left(\frac{\tau_l s + 1}{\alpha \tau_l s + 1}\right),\ 0 < \alpha < 1 \quad \cdots (16)$$

As shown in Fig. 12, Proposal-2 attains the best force tracking performance. Consequently, it achieves better (faster) acceleration.

4. Future trends of DFC

4.1 Extension of practical applications DFC was originally developed for IWM-EV, and then extended to OBM-EV. Until now, almost all the studies in Table 1 have been conducted using a one-seat vehicle or a passenger vehicle (Fig. 13). It is expected that in future, DFC will be extended to cover other applications, such as electric bus, electric truck, car-like-robot with mecanum wheels, and unmanned autonomous electric vehicle. Fujimoto group collaborated with Mitsubishi Motors to investigate DFC for the electric vehicles installed with two-motor-torque difference amplification-torque vectoring differential (TDA-TVD) [20]. Recently, study on DFC for electric truck has been kicked-off by the joint research program between the University of Tokyo and Komatsu Ltd [21] [22].

4.2 Enhanced DFC by advanced parameter estimation Recently, Ueno and Pousseur et al proved the feasibility of road friction estimation for DFC by using an onboard camera with image processing algorithm (Fig. 14) [9]. The algorithm helps the DFC to switch the value of the SL in accordance with high or low friction surface. However, the image processing algorithm [9] still needs time to grow up. At step 5, the algorithm merely assigns for each grid cell a value between [-1, +1]. A value close to -1 represents a road surface (or high friction surface), and a value close to +1 represents a blue-sheet surface (or low friction surface). It is essential to extend the algorithm to cover different road conditions with different values of friction coefficient. To this end, an idea is to combine image processing algorithm with a neural network and a qualified training process.

4.3 DFC based hierarchical decentralized motion control Upper-layer motion control objectives do not limit to yaw-rate and chassis velocity. Therefore, other objectives should be investigated in the future study of DFC. Typical objectives are vehicle body side-slip angle, position/trajectory, and heading angle. Other research trends are:

- Integration of DFC with active steering control for autonomous vehicles: It will be interesting to examine the fault tolerance control of the vehicle system installed with both driving motors and steering motors.

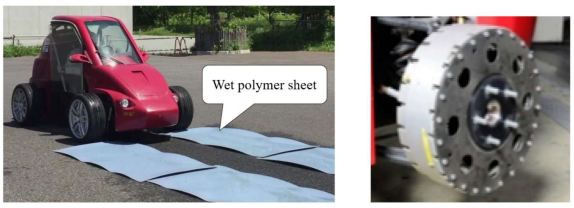

(a) Electric vehicle and low-friction surface. (b) In-wheel-motor.

Fig. 13. DFC experiment of Fujimoto group in Kashiwa Campus.

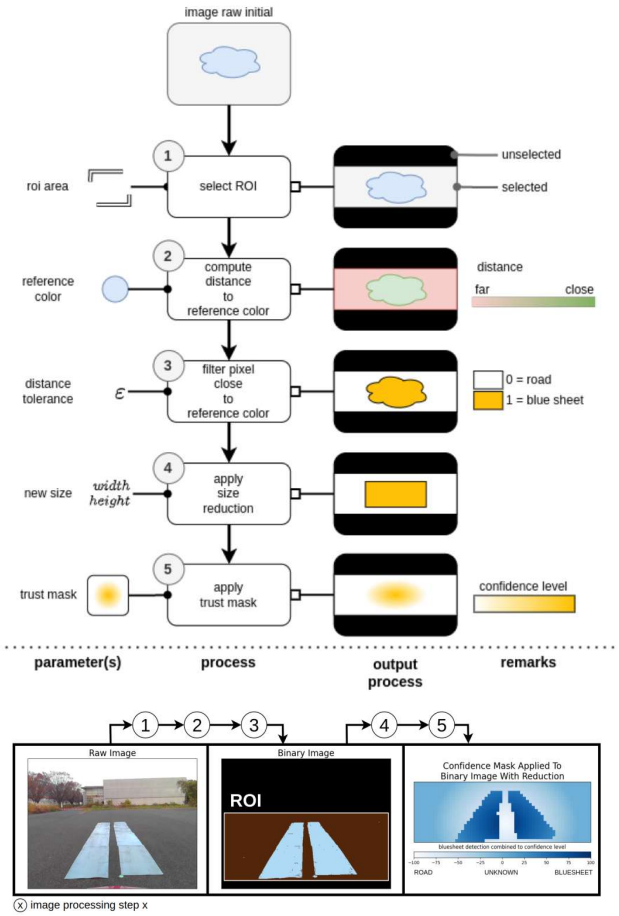

(a) Illustration of image processing pipeline.

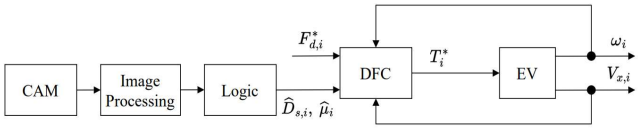

(b) DFC system supported by image processing.

Fig. 14. Onboard camera based DFC control.

- Integration of DFC with artificial intelligence (AI) and machine learning (ML): Model based design is suitable for IWM-EV with relatively simple structure. However, AI/ML could be an option to enhance the control performance of DFC with respect to very complex drivetrains. For instance, vibration suppression of OBM-EV using DFC can be a possible research question.
- Integration of DFC with range extension control: Range extension control is to minimize the motor input power/energy by properly distributing the driving force to each wheel in real time [26]. The optimal distribution ratios are shown to be the function of velocity and acceleration, with the parameter of driving stiffness. Thus, accurate identification of driving stiffness and road friction coefficient would be helpful for both DFC and range extension control purposes.

5. Conclusions

Fifteen years is not a long period, and DFC is still a young fellow in the field of motion control. But fifteen years is enough to confirm that DFC has grown up to overcome the demerit of the traditional traction control approaches. DFC accurately and directly manages the friction between the wheel and road surface. Thus, DFC can be treated as a "local controller" to attain any "global objective" of the vehicle body. It can be expected that DFC will soon be integrated with autonomous driving control, roll control, pitch control, energy management for various types of EVs. DFC will be enhanced by utilizing state of the art in parameter estimation, especially computer vision and machine learning. Considering the EVs driven by multiple motors, advanced control theories would be chosen to guarantee system stability and alleviate the design burden. A brighter future is yet to come with DFC.

References

(1) B.-M. Nguyen, J. P. Trovao, M.-C. Ta, and M. Kawanishi: "Longitudinal Motion Control of Electric Vehicles: Glocal Model and Design Using Passivity," IEEE Vehicular Technology Magazine, Vol.16, Iss.3, pp.75-86 (2021)

(2) Z. He, Q. Shi, Y. Wei, B. Gao, B. Zhu, and L. He: "A Model Predictive Control Approach with Slip ratio Estimation for Electric Motor Antilock Braking of Battery Electric Vehicle," IEEE Transactions on Industrial Electronics, Vol.69, No.9, pp.9225–9234 (2021)

(3) K. Han, M. Choi, B. Lee, and S. B. Choi: "Development of A Traction Control System Using a Special Type of Sliding Mode Controller for Hybrid 4WD Vehicles," IEEE Transactions on Vehicular Technology, Vol.67, No.1, pp. 264–274 (2017)

(4) B.-M. Nguyen, J. P. F. Trovao, and M.-C. Ta: "Double-layer Energy Management for Multi-motor Electric Vehicles," IEEE Transactions on Vehicular Technology, Vol.72, No.7, pp.8623–8635 (2023)

(5) S. Kim, S. H. Yu, and H. Lee: "Traction Control Using a Disturbance Observer for Hybrid Electric Vehicles," International Journal of Automotive Technology, Vol.22, pp.1485–1494 (2021)

(6) J.-S. Hu, D. Yin, Y. Hori, and F.-R. Hu: "Electric Vehicle Traction Control: A New MTTE Methodology," IEEE Industry Applications Magazine, Vol.18, Iss.2, pp.23-31 (2011)

(7) M. Yoshimura and H. Fujimoto: "Driving Torque Control Method for Electric Vehicle with In-Wheel Motors", IEEJ Transactions on Industry Applications, Vol.131, No.5, pp.721-728 (2011)

(8) H. Fuse and H. Fujimoto: "Cornering Force Maximization With Variable Slip Ratio Control for Independent-All-Wheel-Drive Electric Vehicle," IEEE Journal of Emerging and Selected Topics in Industrial Electronics, Vol.4, No. 1, pp.381-388 (2023)

(9) T. Ueno, H. Pousseur, B. M. Nguyen, A. Correa Victorino and H. Fujimoto, "Proposal of On-board Camera-Based Driving Force Control Method for Autonomous Electric Vehicles," IEEE/ASME International Conference on Advanced Intelligent Mechatronics, pp. 424-429 (2023)

(10) K. Maeda, H. Fujimoto, and Y. Hori: "Four-wheel Driving-force Distribution Method for Instantaneous or Split Slippery Roads for Electric Vehicle," Automatika, Vol.54, No.1, pp.103–113 (2013)

(11) T. Ueno, B. -M. Nguyen and H. Fujimoto: "Direct Yaw Moment Control for Electric Vehicles with Variable-Rate-Slip-Ratio-Limiter Based Driving Force Control," IEEE International Conference on Mechatronics, pp.1-6 (2023)

(12) S. Egami and H. Fujimoto: "Range Extension Control System for Electric Vehicles Based on Front and Rear Driving Force Distribution Considering Load Transfer," 37th Annual Conference of the IEEE Industrial Electronics Society, pp. 3852-3857 (2011)

(13) T. Ueno, B.-M. Nguyen and H. Fujimoto, "Driving Force Control for In-Wheel Motor Electric Vehicles with Wheel Speed Limiter and Absolute Stability Analysis," 49th Annual Conference of the IEEE Industrial Electronics Society, pp.1-6, (2023)

(14) T. Ueno, B.-M. Nguyen, S. Nagai and H. Fujimoto, "Wheel Velocity Based Cascade Driving Force Control for Electric Vehicles," IEEE/ASME Transactions on Mechatronics, doi: 10.1109/TMECH.2024.3456151 (2024)

(15) B.-M. Nguyen, T. Ueno, Y. Hosomi, T. Sato, S. Hara and H. Fujimoto, "Basic Study on Wheel Speed Based Driving Force Control for Multi-motor Electric Vehicles with Glocal Stability Analysis," IEEE Vehicle Power and Propulsion Conference, pp.1-6 (2024)

(16) H. Sumiya and H. Fujimoto: "Driving Force Control Method Using Suppression Control of Driving-shaft Vibration for Electric Vehicle with On-board Motor", IEEJ Technical Meeting on Industrial Measurement and Control, p. IIC-12-106 (2012)

(17) J. Amada and H. Fujimoto: "Driving Force Control Method with Resonance Suppression for Drive Shaft of Electric Vehicle with On-board Motor," Joint Technical Meeting on "Industrial Measurement and Control" and "Mechatronics Control," p. IIC-13-003, MEC-13-003 (2013)

(18) H. Fujimoto, T. Miyajima, and J. Amada: "Development of Electric Vehicle with Variable Drive Unit System", International Electric Vehicle Technology Conference & Automotive Power Electronics Japan (2014)

(19) M. Oda, S. Nagai, H. Fujimoto, K. Sato, K. Mizoguchi, N. Takizawa, H. Fujita, K. Yamamoto, and T. Urano: "Evaluation of Vibration Suppression Control for Parallel Shaft e-Axle Using Test Bench System," Spring Conference of Japan Society of Automotive Engineers, (2024)

(20) G. Yu, H. Fuse, H. Fujimoto, K. Sawase, N. Takahashi, R. Takahashi, Y. Okamura, R. Koga: "Feedback Control Design for Drive Shaft Vibration Suppression Based on Frequency Domain Analysis of Two-Input-Two-Output Motor Drive System," 48th Annual Conference of the IEEE Industrial Electronics Society, pp.1-6 (2022)

(21) Y. Hosomi, B.-M. Nguyen, H. Fujimoto, H. Ikeda, and T. Nohara: "Driving Force Control for On-board Motor Electric Vehicles with Adaptive Drivetrain Friction and Phase Stabilization Speed Controller," IEEE International Conference on Advanced Intelligent Mechatronics, pp.1456-1461 (2024)

(22) Y. Hosomi, B.-M. Nguyen, H. Fujimoto, H. Ikeda, and T. Nohara: "Wheel-speed based Driving Force Control for On-board Motor Electric Vehicles with Absolute Stability Analysis and HIL Evaluation," IEEE Vehicle Power and Propulsion Conference, pp.1-6 (2024)

(23) T. Sato, T. Ueno, B.-M Nguyen, H. Fujimoto, and H. Toyota, K. Sawase: "Sideslip Angle Based Variable Slip Ratio Limiter for Direct Yaw Moment Control of Two-Input-Two-Output Motor Vehicles," IEEE International Conference on Advanced Intelligent Mechatronics, pp.1476-1481 (2024).

(24) H. B. Pacejka and E. Bakker: "The Magic Formula Tyre Model," Vehicle System Dynamics, Vol.21, no.S1, pp. 1–18 (1992)

(25) H. K. Khalil: "Nonlinear System," Prentice-Hall (2002).

(26) H. Fujimoto and S. Harada: "Model-Based Range Extension Control System for Electric Vehicles with Front and Rear Driving-Braking Force Distributions," IEEE Transactions on Industrial Electronics, Vol.62, No.5, pp. 3245-3254 (2015).